Ultrafast Imaging of Molecular Chirality with Photoelectron Vortices

Xavier Barcons Planas[1], Andrés Ordóñez[1], Maciej Lewenstein[1,2] and Andrew S. Maxwell[1,3]

[1]*ICFO–Institut de Ciencies Fotoniques, The Barcelona Institute of Science and Technology,*
08860 Castelldefels (Barcelona), Spain
[2]*ICREA, Passeig de Lluís Companys 23, 08010 Barcelona, Spain*
[3]*Department of Physics and Astronomy, Aarhus University, DK-8000 Aarhus C, Denmark*

Ultrafast imaging of molecular chirality is a key step toward the dream of imaging and interpreting electronic dynamics in complex and biologically relevant molecules. Here, we propose a new ultrafast chiral phenomenon exploiting recent advances in electron optics allowing access to the orbital angular momentum of free electrons. We show that strong-field ionization of a chiral target with a few-cycle linearly polarized 800 nm laser pulse yields photoelectron vortices, whose chirality reveals that of the target, and we discuss the mechanism underlying this phenomenon. Our Letter opens new perspectives in recollision-based chiral imaging.

A major goal motivating research in ultrafast science [1,2] is to image and understand electron dynamics in complex systems, such as biologically relevant molecules [3]. However, except for the simplest molecules, interpretation of ultrafast measurements in terms of molecular structure remains extremely challenging [4,5]. Since chirality is both a common and a key structural property of biological molecules [6], the ultrafast imaging of molecular chirality has become a natural objective of ultrafast science during the past decade [7–11]. The current progress in this direction [12] has invariably relied on the Archimedes screw principle: a chiral structure, here the molecular potential, converts the electron rotation induced by the electric field into a linear electron current perpendicular to the rotation plane.

Motivated by progress in the generation and measurement of free-electron vortices [13–18]—free electrons with a helical phase front carrying orbital angular momentum (OAM)—here we propose an alternative and more direct approach to ultrafast imaging of molecular chirality, which does not rely on rotating electric fields. We propose to transfer chirality from the molecule and its initial electronic state directly into the photoelectron wave packet with the help of an intense ultrashort *linearly* polarized IR laser pulse. The strong laser electric field lowers the barrier of the binding potential for a brief period of time, during which the electron is released and accelerated away from the molecular ion. During this process, the chiral shape of the initial electron wave function is imprinted in the three-dimensional phase structure of the released electron wave packet and can be recovered via electron-OAM measurements [see Fig. 1(a)].

The helicity of the electron vortex is given by the projection of its linear momentum $\vec{p}$ on its OAM $\vec{l}$.

Since this helicity is determined by the chirality of the initial wave function, photoelectrons propagating in opposite directions have opposite OAM [see Fig. 1(a)]. We call this effect photoelectron vortex dichroism (PEVD) and quantify it by direct integration of the time-dependent Schrödinger equation for a simple chiral target. Our numerical results show that PEVD is a very promising candidate for monitoring chiral dynamics with subfemtosecond time resolution.

In the following we assume that the fixed nuclei approximation holds and that the vibrational degree of freedom plays a secondary role [19–21]. As usual in strong-field ionization, we will focus on the electronic wave function at the level of the single-active-electron approximation and considering molecular orientation as a parameter.

To describe strong-field ionization from our chiral target, we first employ the plane-wave-momentum transition amplitude,

$$M(\mathbf{p}|\chi^\epsilon) = \lim_{\substack{t_0 \to -\infty \\ t \to \infty}} \langle \psi_\mathbf{p}(t)|U(t,t_0)|\chi^\epsilon(t_0)\rangle, \qquad (1)$$

where $|\chi^\epsilon\rangle$ is the chiral initial state of the target, the superscript $\epsilon = \pm$ indicates the enantiomer, $U(t,t_0) = \hat{T} \exp[\int_{t_0}^t d\tau \hat{H}(\tau)]$ is the time evolution operator (with $\hat{T}$ being the time-ordering operator) corresponding to the Hamiltonian $\hat{H}(\tau) = \hat{p}^2/2 + V(\hat{r}) + r_\parallel E(\tau)$ in the single-active-electron and electric-dipole approximation, and $|\psi_\mathbf{p}\rangle$ describes a continuum state with asymptotic momentum $\mathbf{p}$. Atomic units are used throughout, unless stated otherwise.

For the sake of both simplicity in the numerical implementation and clarity in the interpretation of the numerical results, we take the initial state to be the helical orbital
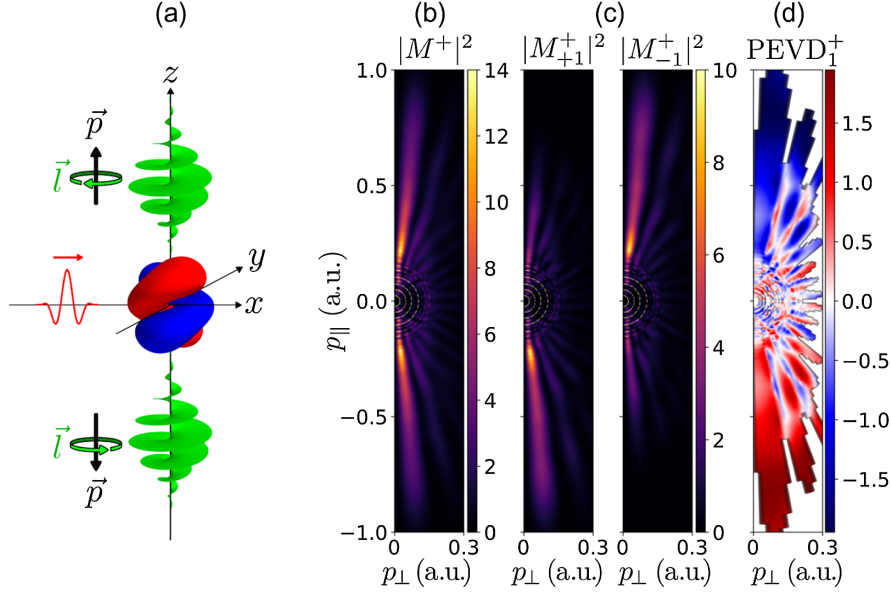
FIG. 1. (a) Photoionization of a chiral target with linearly polarized light produces photoelectron vortices with a helicity that encodes the handedness of the target, thus carrying opposite OAM in opposite propagation directions. The target orbital at the origin shows isosurfaces $\chi^+(\vec{r}) = \pm 10^{-3}$ a.u. [Eq. (2)]. (b) Standard photoelectron spectrum [Eq. (1)] resulting from strong-field ionization of a perfectly aligned chiral target $|\chi^+\rangle$ [Eq. (2)] as a function of the momentum perpendicular and parallel to the laser field. (c) OAM-resolved photoelectron spectra [Eq. (5)] for OAM $l_v = +1$ (left) and $l_v = -1$ (right). (d) Difference of the OAM-resolved spectra normalized by their average [Eq. (7)] for momenta such that $(|M^+_{+1}|^2 + |M^+_{-1}|^2)/2$ is at least 2% of the maximum of (b). All spectra (b)–(d) are in atomic units and were obtained for a peak intensity $I = 10^{14}$ W/cm^2 ($U_p = 0.22$ a.u.), carrier frequency $\omega = 0.057$ a.u. ($\lambda = 800$ nm), $N = 2$ cycles [Eq. (6)], and ionization potential $I_p = 0.579$ a.u. of argon. All results were averaged over the carrier-envelope phase δ and over orientations of the target corresponding to rotations of Eq. (2) around z.

shown in Fig. 1(a), which is given by a superposition of hydrogenic states according to [22,23]

$$|\chi^\epsilon\rangle = \frac{|\chi^\epsilon_1\rangle + |\chi^\epsilon_{-1}\rangle}{\sqrt{2}},\qquad(2)$$

with

$$|\chi^\epsilon_m\rangle = \frac{i|4f_m\rangle + \mathrm{sgn}(\epsilon m)|4d_m\rangle}{\sqrt{2}}.\qquad(3)$$

Here, $|n\ell_m\rangle$ denotes the hydrogenic state with principal, orbital, and magnetic quantum numbers n, ℓ, and m, respectively. Orbitals with similar helical shapes are common among chiral allenes [24,25], an important type of compound in organic chemistry [24,26].

We use an effective charge $Z = 4\sqrt{2I_p}$ to fix the ionization potential of $|\chi^\epsilon\rangle$ to that of argon $I_p = 0.579$ a.u., a well-studied target in strong-field ionization. The enantiomers $|\chi^+\rangle$ and $|\chi^-\rangle$ are related to each other by reflection in the xz plane. The decomposition of $|\chi^\epsilon\rangle$ into its azimuthal angular momentum components $|\chi^\epsilon_{m=\pm1}\rangle$ in Eq. (3) reveals an enantiosensitive correlation [27] between the sign of m (rotation around z) and the relative phase between the d and f components (motion or asymmetry along z) in $|\chi^\epsilon_{\pm1}\rangle$. Such a correlation between rotation and motion along the rotation

axis is not a peculiarity of these states, but rather a quintessential feature of chiral objects (e.g., a corkscrew). As we discuss below, this general feature is at the heart of PEVD.

In order to model the photoelectron OAM in strong-field ionization we will expand the transition amplitude in terms of vortex states with a well-defined OAM l_v; these take the form [13]

$$\psi_{l_v}(\mathbf{r}) \propto J_{l_v}(p_\perp r_\perp)e^{il_v\phi_r}e^{ip_\parallel r_\parallel},\qquad(4)$$

where $J_{l_v}(p_\perp r_\perp)$ is the Bessel function of the first kind and $(r_\perp, r_\parallel, \phi_r)$ and $(p_\perp, p_\parallel, \phi_p)$ are the cylindrical coordinates of $\mathbf{r}$ and $\mathbf{p}$, respectively. The OAM-resolved transition amplitude, in terms of the transition amplitude [Eq. (1)], yields

$$M_{l_v}(p_\parallel, p_\perp|\chi^\epsilon) = \frac{i^{l_v}}{2\pi}\int_{-\pi}^{\pi} d\phi_p e^{-il_v\phi_p}M(\mathbf{p}|\chi^\epsilon)$$
$$= i^{l_v}M(\mathbf{p}|\chi^\epsilon_{l_v})|_{\phi_p=0}.\qquad(5)$$

The final line exploits the conservation of azimuthal angular momentum, when using a linear field aligned as in Fig. 1(a), so that the photoelectron OAM will only include contributions from the bound state with $m = l_v$. In the following, we use the shorthand notation $M^\epsilon \equiv M(p_\parallel, p_\perp|\chi^\epsilon)$ for the

plane-wave amplitude and $M_{l_v}^\epsilon \equiv M_{l_v}(p_\parallel, p_\perp|\chi^\epsilon)$ for the OAM-resolved amplitude.

We will employ a two-cycle laser field linearly polarized along the z axis; see Fig. 1(a). PEVD also occurs for longer pulses, but the interpretation is simplest for short pulses, where recollision of the electron with the parent ion is suppressed. The electric field is given by $\mathbf{E}(t) = -\partial_t\mathbf{A}(t)$ and the vector potential can be written as

$$\mathbf{A}(t) = A_0\sin^2\left(\frac{\omega t}{2N}\right)\cos\left(\omega t + \delta\right)\hat{\mathbf{e}}_z. \quad (6)$$

Here, $A_0 = 2\sqrt{U_p}$, where U_p is the ponderomotive energy, ω the laser frequency, N the number of laser cycles, and δ the carrier-envelope phase (CEP). In order to avoid asymmetries in the angular distributions resulting from the laser field, all results will be averaged over the CEP δ.

We use QPROP to compute the OAM-resolved momentum distribution via Eq. (5). QPROP [28] enables the efficient simulation of a single active electron bound in a spherically symmetric potential, interacting with an intense laser field. As previously stated, we utilize a Coulomb potential with an effective charge $Z = 4\sqrt{2I_p}$, so that the binding energy is equal to $-I_p$.

In Fig. 1, we demonstrate the enantiosensitive asymmetry present in PEVD. Figure 1(a) summarizes the key finding of this Letter, namely that photoionization of a chiral target with linearly polarized light yields photoelectron vortices whose helicity encodes the handedness of the chiral target. In terms of OAM, this means that photoelectrons emitted in opposite directions carry opposite OAM. This effect is quantified in the remaining panels, which display CEP-averaged momentum distributions, computed using QPROP for an aligned [29] target $|\chi^+\rangle$. For the sake of comparison, Fig. 1(b) shows the usual plane-wave photoelectron momentum distribution [see Eq. (1)]. The signal, which is mostly located near the polarization axis, is completely symmetric with respect to $p_\parallel$ and is not enantiosensitive. Figure 1(c) shows the OAM-resolved momentum distribution [Eq. (5)] for OAM $l_v = +1$ ($|M_{+1}^+|^2$) and $l_v = -1$ ($|M_{-1}^+|^2$), respectively. Now the emission displays an OAM-dependent asymmetry with respect to $p_\parallel$, such that photoelectrons with positive (negative) OAM are emitted preferentially in the negative (positive) $p_\parallel$ direction.

To quantify this OAM dependence we proceed as usual in other chiro-optical techniques and define PEVD as the difference between the signals corresponding to opposite OAM normalized by their average,

$$\text{PEVD}_{l_v}^\epsilon \equiv 2\frac{|M_{l_v}^\epsilon|^2 - |M_{-l_v}^\epsilon|^2}{|M_{l_v}^\epsilon|^2 + |M_{-l_v}^\epsilon|^2} = 2\frac{|M_{l_v}^\epsilon|^2 - |M_{l_v}^{-\epsilon}|^2}{|M_{l_v}^\epsilon|^2 + |M_{l_v}^{-\epsilon}|^2}. \quad (7)$$

The second equality, which explicitly shows the enantiosensitive character of this measure ($\text{PEVD}_{l_v}^{-\epsilon} = -\text{PEVD}_{l_v}^\epsilon$),

follows from the property $|M_{-l_v}^{-\epsilon}|^2 = |M_{l_v}^\epsilon|^2$, which we have verified in our calculations and is required by symmetry. Indeed, mirror reflection of the setup shown in Fig. 1(a), in the xz plane, inverts the enantiomer as well as the OAM of each vortex. In Fig. 1(d) we can see that PEVD_1^+ reaches values approaching the theoretical extremes of $\pm 200\%$, showing that it is an extremely sensitive measure of molecular chirality. Note that (i) we made no attempt to maximize this value by tweaking the initial wave function and (ii) an actual molecular electronic state will contain, in general, several m components, leading to several l_v values of the photoelectron OAM, and thus to several $\text{PEVD}_{l_v}^\epsilon$ distributions, i.e., multiple enantiosensitive observables.

The $p_\parallel$ asymmetry in Fig. 1(c) derives from conservation of OAM, which enforces that only the bound-state component $|\chi_m^+\rangle$ [Eq. (3)] with $m = l_v$ contributes to photoelectrons with OAM l_v [Eq. (5)]. The z asymmetry of this single-OAM component $|\chi_{l_v}^+\rangle$ is imprinted on the photoelectron vortex momentum distribution $|M_{l_v}^+|^2$. Because of the chiral correlation between rotation around z and motion or asymmetry along z in $|\chi_m^\epsilon\rangle$, the z asymmetry of $|\chi_{l_v}^+\rangle$ is opposite for opposite values of l_v [Eq. (3)], and thus $|M_{l_v}^+|^2$ and $|M_{-l_v}^+|^2$ display opposite asymmetries with respect to $p_\parallel$.

While virtually perfect molecular alignment is possible [30] and we expect PEVD to be maximal in this case, we consider also PEVD for a modest degree of alignment. The inclusion of different orientations leads to contributions of orbitals with $m \in [-3, 3]$, and correspondingly, $l_v \in [-3, 3]$. For more details on orientation averaging, see the Supplemental Material [31]. The orientation-averaged CEP-averaged momentum distributions calculated with QPROP are shown in Fig. 2. The distribution $P(\beta) = 3\cos^2(\beta)$ leads to target orientation such that $\langle\cos^2(\beta)\rangle = 0.6$, which is routinely achievable in experiments by an alignment prepulse [32]. Note that β is the angle between the z axes of the molecular and laboratory frames [33]. As before, in Fig. 2(a) we plot the plane-wave momentum distribution, which remains symmetric, but is now averaged over molecular orientations, introducing orbitals with additional m values, in particular $m = 0$, that leads to a strong signal along the $p_\parallel$ axis. In Figs. 2(b) and 2(d), the OAM-resolved momentum distribution is plotted for $l_v = \pm 1$ and $l_v = \pm 2$, respectively. Figure 2(b) is equivalent to Fig. 1(c): the partial alignment leads to some reduction in the asymmetry, such that $|\langle\text{PEVD}_1^+\rangle|$, Fig. 2(c), peaks at 50%. On the other hand, the higher OAM $l_v = \pm 2$ in Fig. 2(d) allows for a larger asymmetry, as the initial state $|\chi_2^\pm\rangle$ exhibits even more bias in the momentum distribution, enabling $|\langle\text{PEVD}_2^+\rangle| \approx 120\%$ to be achieved in Fig. 2(e). The signal of $\langle|M_{\pm2}^+|^2\rangle$ is lower than that of $\langle|M_{\pm1}^+|^2\rangle$, but a sizable region in momentum is larger than 2% of the peak of $\langle|M^+|^2\rangle$, and thus could be reasonably measured. We do not plot $\langle|M_0^+|^2\rangle$ or $\langle|M_{\pm3}^+|^2\rangle$ as they are both
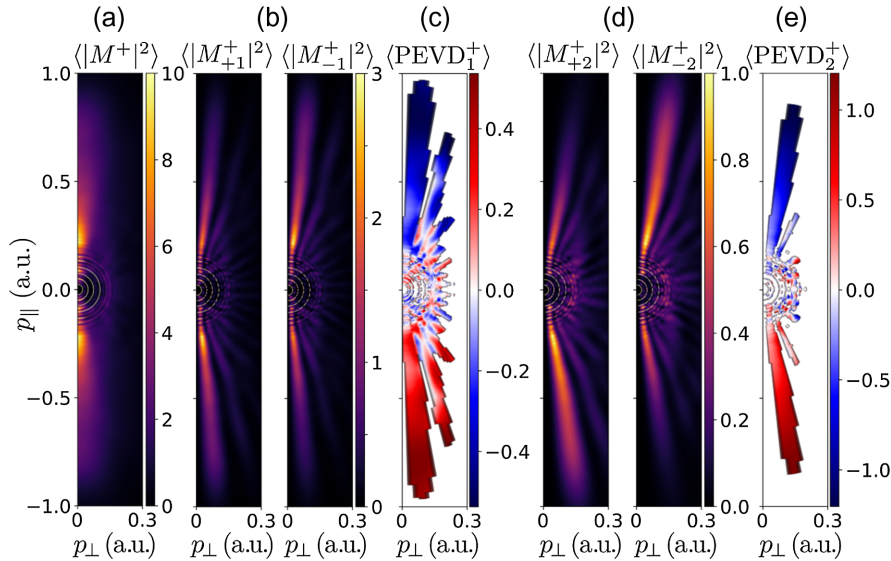
FIG. 2. Photoelectron spectra as in Fig. 1 but for a partially aligned chiral target with a distribution of orientations given by $P(\beta) = 3\cos^2(\beta)$ ($\langle\cos^2\beta\rangle = 0.6$); see the Supplemental Material [31] for details.

symmetric and not enantiosensitive, which is because the photoelectron will derive from a single symmetrical s and f state, respectively.

Like most chiral effects [11,14,34–38], we expect PEVD to occur even for randomly oriented samples. However, reproducing such behavior with photoelectrons requires including the effect of the anisotropy of the molecular potential on the continuum states, which can be interpreted as a higher-order contribution to the continuum states (see, e.g., Ref. [39]).

We have also confirmed that the enantiosensitive asymmetry may be replicated by the strong-field approximation (SFA); see Supplemental Material for details [31]. The SFA uses an intuitive quantum orbit formalism; see, e.g., Refs. [40–42]. Within the SFA the asymmetry can also be partially attributed to interference between wave packets that tunnel ionize from either side of the target. For the short pulses used here such interference does not play a role, but it is relevant for longer laser pulses, where it may allow for holographic chiral imaging. In Fig. 1 of the Supplemental Material [31] we show PEVD for a ten-cycle pulse, where rich features due to recollision can be observed. The detailed mechanisms behind these features could be investigated by a "Coulomb-corrected" quantum-orbit model such as the Coulomb quantum-orbit strong-field approximation [43–45].

In summary, we have showcased the newly discovered effect—photoelectron vortex dichroism, which leads to a large asymmetry in the orbital-angular-momentum-resolved photoelectron momentum distributions for a chiral target subjected to a strong linearly polarized laser field. This asymmetry is the manifestation of a laser-assisted transfer of chirality from the bound orbital to the photoelectron vortex wave packet, which provides an intrinsically chiral

observable. The emergence of PEVD reflects the fact that chiral molecules are a natural source of electron vortices that relies neither on the spin angular momentum of the photon nor on the net OAM of the initial state. The high enantio-sensitivity of PEVD was demonstrated numerically using the time-dependent Schrödinger equation solver QPROP [28], for aligned and partially aligned targets. The enantio-sensitivity of the OAM asymmetry in PEVD is most clearly visible after averaging out the CEP asymmetry induced by the laser pulse and provides a robust experimental observable. Similarly to other chiral effects such as photoelectron circular dichroism [46], we expect PEVD to occur also in randomly oriented samples and furthermore to be a "universal" effect occurring across all photoionization regimes.

In contrast to most electric-dipole chiral effects [47], which rely on circular [49] or on combinations of several linearly polarized fields [11,37,38,50], PEVD relies only on a single beam of linearly polarized light, which is possible thanks to the chiral character of the observable—the OAM helicity [51]. This is an important experimental advantage, in particular when using (broadband and short-wavelength) attosecond pulses, where we also expect PEVD to occur and where the polarization control required by other chiral effects is complicated by lossy and dispersive optics [53]. More importantly, in the strong-field regime linearly polarized light allows for recollision, which leads to processes such as high-harmonic generation [54], high-order above-threshold ionization [41], nonsequential double ionization [55,56], laser-induced electron diffraction [57], and photo-electron holography [58]. Thus, PEVD sets the stage for the study of the role of the electron OAM and the opportunities it offers in recollision-based ultrafast chiral imaging.

Another key aspect of PEVD is that while the spin angular momentum of the photon is strictly limited to -1

and 1, the OAM of the photoelectron is limited only by the complexity of the initial wave function and can take any integer value, thus yielding a rich array of enantiosensitive observables.

To observe PEVD in experiment requires, in the simplest case, the counting of photoelectrons traveling in one direction along the laser field polarization axis and measurement of the OAM (and thus the associated helicity). A lot of activity in the field of electron optics has resulted in an increasing variety of methods (inspired by their analogs in optics) for the measurement of the OAM of an electron wave. These range from simply diffracting the electron wave through a knife edge [59], to mode conversion with astigmatic lenses [60], and very effective state-of-the-art OAM sorting using conformal mapping [61,62], among others (see Refs. [13,63] for reviews). This variety of methods has built upon the electron optics found in transmission electron microscopes (TEMs), and thus we propose to observe PEVD by using chiral molecules as a laser-triggered electron source [64] in a TEM already fitted with an OAM measurement stage (see Supplemental Material for details [31]).

The data and plotting scripts for all figures used in this manuscript is freely available on a Zenodo database [65]. The code written for this manuscript has been made open source and is available as a release on Zenodo [66] and the repository is on GitHub [67].

[1] P. B. Corkum and F. Krausz, Attosecond science, Nat. Phys. 3, 381 (2007).

[2] F. Krausz and M. Ivanov, Attosecond physics, Rev. Mod. Phys. 81, 163 (2009).

[3] F. Calegari, D. Ayuso, A. Trabattoni, L. Belshaw, S. De Camillis, S. Anumula, F. Frassetto, L. Poletto, A. Palacios, P. Decleva, J. B. Greenwood, F. Martin, and M. Nisoli, Ultrafast electron dynamics in phenylalanine initiated by attosecond pulses, Science 346, 336 (2014).

[4] S. R. Leone, C. W. McCurdy, J. Burgdörfer, L. S. Cederbaum, Z. Chang, N. Dudovich, J. Feist, C. H. Greene, M. Ivanov, R. Kienberger, U. Keller, M. F. Kling, Z.-H. Loh, T. Pfeifer, A. N. Pfeiffer, R. Santra, K. Schafer, A. Stolow, U. Thumm, and M. J. J. Vrakking, What will it take to observe processes in 'real time'?, Nat. Photonics 8, 162 (2014).

[5] J. Xu, C. I. Blaga, P. Agostini, and L. F. DiMauro, Time-resolved molecular imaging, J. Phys. B 49, 112001 (2016).

[6] W. A. Bonner, Chirality and life, Origins Life Evol. Biosphere 25, 175 (1995).

[7] R. Cireasa, A. E. Boguslavskiy, B. Pons, M. C. H. Wong, D. Descamps, S. Petit, H. Ruf, N. Thiré, A. Ferré, J. Suarez, J. Higuet, B. E. Schmidt, A. F. Alharbi, F. Légaré, V. Blanchet, B. Fabre, S. Patchkovskii, O. Smirnova, Y. Mairesse, and V. R. Bhardwaj, Probing molecular chirality on a sub-femtosecond timescale, Nat. Phys. 11, 654 (2015).

[8] S. Beaulieu, A. Comby, A. Clergerie, J. Caillat, D. Descamps, N. Dudovich, B. Fabre, R. Géneaux, F. Légaré, S. Petit, B. Pons, G. Porat, T. Ruchon, R. Taïeb, V. Blanchet, and Y. Mairesse, Attosecond-resolved photoionization of chiral molecules, Science 358, 1288 (2017).

[9] D. Baykusheva and H. J. Wörner, Chiral Discrimination through Bielliptical High-Harmonic Spectroscopy, Phys. Rev. X 8, 031060 (2018).

[10] S. Rozen, A. Comby, E. Bloch, S. Beauvarlet, D. Descamps, B. Fabre, S. Petit, V. Blanchet, B. Pons, N. Dudovich, and Y. Mairesse, Controlling Subcycle Optical Chirality in the Photoionization of Chiral Molecules, Phys. Rev. X 9, 031004 (2019).

[11] D. Ayuso, O. Neufeld, A. F. Ordonez, P. Decleva, G. Lerner, O. Cohen, M. Ivanov, and O. Smirnova, Synthetic chiral light for efficient control of chiral light–matter interaction, Nat. Photonics 13, 866 (2019).

[12] D. Ayuso, A. F. Ordonez, and O. Smirnova, Ultrafast chirality: The road to efficient chiral measurements, Phys. Chem. Chem. Phys. 24, 26962 (2022).

[13] K. Y. Bliokh, I. P. Ivanov, G. Guzzinati, L. Clark, R. Van Boxem, A. Béché, R. Juchtmans, M. A. Alonso, P. Schattschneider, F. Nori, and J. Verbeeck, Theory and applications of free-electron vortex states, Phys. Rep. 690, 1 (2017).

[14] A. Asenjo-Garcia and F. J. García de Abajo, Dichroism in the Interaction Between Vortex Electron Beams, Plasmons, and Molecules, Phys. Rev. Lett. **113**, 066102 (2014).

[15] R. Juchtmans, A. Béché, A. Abakumov, M. Batuk, and J. Verbeeck, Using electron vortex beams to determine chirality of crystals in transmission electron microscopy, Phys. Rev. B **91**, 094112 (2015).

[16] A. S. Maxwell, G. S. J. Armstrong, M. F. Ciappina, E. Pisanty, Y. Kang, A. C. Brown, M. Lewenstein, and C. Figueira de Morisson Faria, Manipulating twisted electrons in strong-field ionization, Faraday Discuss. **228**, 394 (2021).

[17] Y. Kang, E. Pisanty, M. Ciappina, M. Lewenstein, C. Figueira de Morisson Faria, and A. S. Maxwell, Conservation laws for electron vortices in strong-field ionisation, Eur. Phys. J. D **75**, 199 (2021).

[18] A. S. Maxwell, L. B. Madsen, and M. Lewenstein, Entanglement of orbital angular momentum in non-sequential double ionization, Nat. Commun. **13**, 4706 (2022).

[19] S. Petretti, Y. V. Vanne, A. Saenz, A. Castro, and P. Decleva, Alignment-Dependent Ionization of N_2, O_2, and CO_2 in Intense Laser Fields, Phys. Rev. Lett. **104**, 223001 (2010).

[20] P. Sándor, V. Tagliamonti, A. Zhao, T. Rozgonyi, M. Ruckenbauer, P. Marquetand, and T. Weinacht, Strong Field Molecular Ionization in the Impulsive Limit: Freezing Vibrations with Short Pulses, Phys. Rev. Lett. **116**, 063002 (2016).

[21] A. D. Müller, E. Kutscher, A. N. Artemyev, and P. V. Demekhin, Photoelectron circular dichroism in the multiphoton ionization by short laser pulses. III. Photoionization of fenchone in different regimes, J. Chem. Phys. **152**, 044302 (2020).

[22] A. F. Ordonez and O. Smirnova, Propensity rules in photoelectron circular dichroism in chiral molecules. i. chiral hydrogen, Phys. Rev. A **99**, 043416 (2019).

[23] A. F. Ordonez and O. Smirnova, Propensity rules for photoelectron circular dichroism in strong field ionization of chiral molecules, Phys. Chem. Chem. Phys. **24**, 5720 (2022).

[24] C. H. Hendon, D. Tiana, A. T. Murray, D. R. Carbery, and A. Walsh, Helical frontier orbitals of conjugated linear molecules, Chem. Sci. **4**, 4278 (2013).

[25] W. Bro-Jørgensen, M. H. Garner, and G. C. Solomon, Quantification of the helicity of helical molecular orbitals, J. Phys. Chem. A **125**, 8107 (2021).

[26] R. K. Neff and D. E. Frantz, Recent applications of chiral allenes in axial-to-central chirality transfer reactions, Tetrahedron **71**, 7 (2015).

[27] For $\epsilon = +$, m and $\text{sgn}(\epsilon m)$ have the same sign. For $\epsilon = -$, m and $\text{sgn}(\epsilon m)$ have opposite signs.

[28] V. Tulsky and D. Bauer, QPROP with faster calculation of photoelectron spectra, Comput. Phys. Commun. **251**, 107098 (2020); V. Mosert and D. Bauer, Photoelectron spectra with QPROP and t-surff, Comput. Phys. Commun. **207**, 452 (2016).

[29] We average over all target orientations resulting from a rotation of Eq. (2) around the z axis followed by a rotation by either 0 or π radians around the y axis.

[30] L. Holmegaard, J. H. Nielsen, I. Nevo, H. Stapelfeldt, F. Filsinger, J. Küpper, and G. Meijer, Laser-Induced Alignment and Orientation of Quantum-State-Selected Large Molecules, Phys. Rev. Lett. **102**, 023001 (2009).

[31] See Supplemental Material at http://link.aps.org/supplemental/10.1103/PhysRevLett.129.233201 for further information on the strong-field approximation, derivation of the length gauge bound-state prefactor, and orientation averaging.

[32] H. Stapelfeldt and T. Seideman, Aligning molecules with strong laser pulses, Rev. Mod. Phys. **75**, 543 (2003).

[33] D. M. Brink and G. R. Satchler, *Angular Momentum*, 2nd ed. (Clarendon Press, Oxford, 1968).

[34] N. Berova, P. L. Polavarapu, K. Nakanishi, and R. W. Woody, *Comprehensive Chiroptical Spectroscopy* (Wiley, Hoboken, NJ, 2012).

[35] A. F. Ordonez, Chiral measurements in the electric-dipole approximation, Ph.D. thesis, Technische Universität Berlin, 2019, 10.14279/depositonce-9677.

[36] M. H. M. Janssen and I. Powis, Detecting chirality in molecules by imaging photoelectron circular dichroism, Phys. Chem. Chem. Phys. **16**, 856 (2014).

[37] P. Fischer and F. Hache, Nonlinear optical spectroscopy of chiral molecules, Chirality **17**, 421 (2005).

[38] D. Patterson and J. M. Doyle, Sensitive Chiral Analysis via Microwave Three-Wave Mixing, Phys. Rev. Lett. **111**, 023008 (2013).

[39] I. Dreissigacker and M. Lein, Photoelectron circular dichroism of chiral molecules studied with a continuum-state-corrected strong-field approximation, Phys. Rev. A **89**, 053406 (2014).

[40] L. Keldysh, Ionization in the field of a strong electromagnetic wave, Sov. Phys. JETP **20**, 1307 (1965); F. H. Faisal, Multiple absorption of laser photons by atoms, J. Phys. B **6**, L89 (1973); H. R. Reiss, Effect of an intense electromagnetic field on a weakly bound system, Phys. Rev. A **22**, 1786 (1980).

[41] W. Becker, F. Grasbon, R. Kopold, D. Milošević, G. Paulus, and H. Walther, Above-threshold ionization: From classical features to quantum effects, Adv. At. Mol. Opt. Phys. **48**, 35 (2002).

[42] K. Amini, J. Biegert, F. Calegari, A. Chacón, M. F. Ciappina, A. Dauphin, D. K. Efimov, C. Figueira de Morisson Faria, K. Giergiel, P. Gniewek *et al.*, Symphony on strong field approximation, Rep. Prog. Phys. **82**, 116001 (2019).

[43] A. S. Maxwell, A. Al-Jawahiry, T. Das, and C. Figueira de Morisson Faria, Coulomb-corrected quantum interference in above-threshold ionization: Working towards multitrajectory electron holography, Phys. Rev. A **96**, 023420 (2017).

[44] A. S. Maxwell and C. Figueira de Morisson Faria, Coulomb-free and Coulomb-distorted recolliding quantum orbits in photoelectron holography, J. Phys. B **51**, 124001 (2018).

[45] A. S. Maxwell, A. Al-Jawahiry, X. Y. Lai, and C. Figueira de Morisson Faria, Analytic quantum-interference conditions in Coulomb corrected photoelectron holography, J. Phys. B **51**, 044004 (2018).

[46] S. Beaulieu, A. Ferré, R. Géneaux, R. Canonge, D. Descamps, B. Fabre, N. Fedorov, F. Légaré, S. Petit, T. Ruchon, V Blanchet, Y. Mairesse, and B. Pons, Universality

of photoelectron circular dichroism in the photoionization of chiral molecules, New J. Phys. **18**, 102002 (2016).

[47] The only (partial) exception we are aware of is Ref. [48], where linear polarization is used but nevertheless turned into elliptical polarization via tight focusing in the interaction region.

[48] D. Ayuso, A. F. Ordonez, M. Ivanov, and O. Smirnova, Ultrafast optical rotation in chiral molecules with ultrashort and tightly focused beams, Optica **8**, 1243 (2021).

[49] B. Ritchie, Theory of the angular distribution of photoelectrons ejected from optically active molecules and molecular negative ions, Phys. Rev. A **13**, 1411 (1976).

[50] P. V. Demekhin, A. N. Artemyev, A. Kastner, and T. Baumert, Photoelectron Circular Dichroism with Two Overlapping Laser Pulses of Carrier Frequencies ω and 2ω Linearly Polarized in Two Mutually Orthogonal Directions, Phys. Rev. Lett. **121**, 253201 (2018).

[51] The OAM is a pseudovector, which with the propagation direction provides an inherently chiral observable, in contrast to the vector character of the usual electric-dipole chiral observables [52].

[52] A. F. Ordonez and O. Smirnova, Generalized perspective on chiral measurements without magnetic interactions, Phys. Rev. A **98**, 063428 (2018).

[53] P.-C. Huang, C. Hernández-García, J.-T. Huang, P.-Y. Huang, C.-H. Lu, L. Rego, D. D. Hickstein, J. L. Ellis, A. Jaron-Becker, A. Becker, S.-D. Yang, C. G. Durfee, L. Plaja, H. C. Kapteyn, M. M. Murnane, A. H. Kung, and M.-C. Chen, Polarization control of isolated high-harmonic pulses, Nat. Photonics **12**, 349 (2018).

[54] M. Lewenstein, P. Balcou, M. Y. Ivanov, A. L'Huillier, and P. B. Corkum, Theory of high-harmonic generation by low-frequency laser fields, Phys. Rev. A **49**, 2117 (1994).

[55] C. Figueira de Morisson Faria and X. Liu, Electron–electron correlation in strong laser fields, J. Mod. Opt. **58**, 1076 (2011).

[56] W. Becker, X. J. Liu, P. J. Ho, and J. H. Eberly, Theories of photoelectron correlation in laser-driven multiple atomic ionization, Rev. Mod. Phys. **84**, 1011 (2012).

[57] T. Zuo, A. D. Bandrauk, and P. B. Corkum, Laser-induced electron diffraction: A new tool for probing ultrafast molecular dynamics, Chem. Phys. Lett. **259**, 313 (1996).

[58] C. Figueira de Morisson Faria and A. S. Maxwell, It is all about phases: Ultrafast holographic photoelectron imaging, Rep. Prog. Phys. **83**, 034401 (2020).

[59] G. Guzzinati, L. Clark, A. Béché, and J. Verbeeck, Measuring the orbital angular momentum of electron beams, Phys. Rev. A **89**, 025803 (2014).

[60] P. Schattschneider, M. Stöger-Pollach, and J. Verbeeck, Novel Vortex Generator and Mode Converter for Electron Beams, Phys. Rev. Lett. **109**, 084801 (2012).

[61] V. Grillo, A. H. Tavabi, F. Venturi, H. Larocque, R. Balboni, G. C. Gazzadi, S. Frabboni, P. H. Lu, E. Mafakheri, F. Bouchard, R. E. Dunin-Borkowski, R. W. Boyd, M. P. J. Lavery, M. J. Padgett, and E. Karimi, Measuring the orbital angular momentum spectrum of an electron beam, Nat. Commun. **8**, 15536 (2017).

[62] A. H. Tavabi, P. Rosi, E. Rotunno, A. Roncaglia, L. Belsito, S. Frabboni, G. Pozzi, G. C. Gazzadi, P.-H. Lu, R. Nijland, M. Ghosh, P. Tiemeijer, E. Karimi, R. E. Dunin-Borkowski, and V. Grillo, Experimental Demonstration of an Electrostatic Orbital Angular Momentum Sorter for Electron Beams, Phys. Rev. Lett. **126**, 094802 (2021).

[63] S. Lloyd, M. Babiker, G. Thirunavukkarasu, and J. Yuan, Electron vortices: Beams with orbital angular momentum, Rev. Mod. Phys. **89**, 035004 (2017).

[64] P. Baum, On the physics of ultrashort single-electron pulses for time-resolved microscopy and diffraction, Chem. Phys. **423**, 55 (2013).

[65] X. B. Planas, A. Ordóñez, M. Lewenstein, and A. S. Maxwell, Ultrafast Imaging of Molecular Chirality with Photoelectron Vortices (2022), 10.5281/zenodo.6939947.

[66] X. B. Planas, A. Ordóñez, M. Lewenstein, and A. S. Maxwell, Asmaxwell/SFA_OAM_Linear: Ultrafast imaging of molecular chirality with photoelectron vortices—SFA source code (2022), 10.5281/zenodo.6940297.

[67] A. S. Maxwell and X. B. Planas, SFA OAM Linear (2022), https://github.com/asmaxwell/SFA_OAM_Linear.